Compact Computer Model of Rabbit Atrioventricular Node with Autonomic Nervous System Control

Maxim Ryzhii[1], Elena Ryzhii[2]

[1] University of Aizu, Aizu-Wakamatsu, Japan
[2] Fukushima Medical University, Fukushima, Japan

Abstract

We present an updated version of our compact multifunctional computer model of the rabbit AV node. In addition to the previous version, the model includes autonomic nervous system control of AV node conduction. The combined influence of sympathetic and parasympathetic tones is manifested in changes in the atrial-His bundle conduction time and regular sinus rhythm, the onset and spontaneous termination of atrioventricular nodal reciprocal tachycardia, and changes in filtering function during atrial fibrillation.

1. Introduction

The atrioventricular (AV) node transmits signals from the atria to the ventricles, playing a vital role in synchronizing atrial and ventricular contractions by providing conduction delay and protecting the ventricles from atrial tachyarrhythmias. The electrophysiological processes inside the AV node are not completely clear, and their study through experiments is rather difficult. At the same time, the number of computer models of the AV node with dual pathways is limited [1–3].

Recently, we developed a compact multifunctional computer model of the rabbit AV node [4]. The model includes a simplified sinoatrial node (SN), dual [fast (FP) and slow (SP)] pathway AV node structure, AV nodal pacemaker, and proximal His bundle. The model closely reproduces experimentally obtained anterograde and retrograde conduction curves [5] and allows visualization of FP and SP conduction in the form of ladder diagrams, providing deeper insight into the interaction of AV nodal pathways.

The updated model incorporates the autonomic nervous system (ANS) control and allows simulation of the combined effect of sympathetic and parasympathetic parts of ANS on AV nodal conduction. This effect manifests in changes in atrial-His bundle conduction time and regular sinus rhythm, the onset and spontaneous termination of atrioventricular nodal reentrant tachycardia (AVNRT), and alteration of filtering function in atrial fibrillation (AF) [6].

2. Model

The scheme of the compact AV node model is shown in Fig. 1(a). Each model cell is described by Aliev-Panfilov (A-P) model [7] given by the following set of ordinary differential equations

$$\dot{V} = c[kV(V-a_1)(1-V) - rV] + I^{coupl} + I^{stim}, \quad (1)$$

$$\dot{r} = c[\epsilon_0 + r\mu_1/(V+\mu_2)][-r - kV(V-a_2-1)], \quad (2)$$

where V is the dimensionless transmembrane potential, r is the gate variable, c is the time scaling coefficient, k is the parameter controlling the magnitude of the transmembrane current. Parameters ϵ_0, a_1, a_2, μ_1, and μ_2 determine the conduction characteristics of tissue, $a_1 > 0$ represents the excitation threshold of quiescent excitable cells, while $a_1 < 0$ sets the intrinsic oscillation frequency of the pacemaking cells [8]. The parameter values were similar to that used in [4] and are based on rabbit experimental data [5]. The intercellular coupling term I^{coupl} accounts for the coupling asymmetry, and I^{stim} is the stimulation current applied to atrial cells [Fig. 1(a)].

According to the clinical and experimental data [9], the enhanced sympathetic tone may cause AVNRT onset, while the increased activity of parasympathetic tone slowing electrical conduction in the AV node may terminate the tachycardia [10]. With the S1S2 protocol application, the reentrant activity appears in the range of S2 test pulses shorter than FP effective refractory period (ERP) [11, 12].

In an attempt to incorporate the ANS control, we first examined how the A-P model parameters k, ε_0, μ_1, and μ_2 affect AV nodal conduction time by multiplying each parameter on a coefficient γ. Under parasympathetic dominance, γ was expected to slow conduction in the SP and FP, suppressing periodic oscillations in the AV ring (AVNRT) and reducing the intrinsic frequency of pacemaker cells.

The effect of the A-P model parameters variation on the AV nodal conduction curves and SN intrinsic rate is

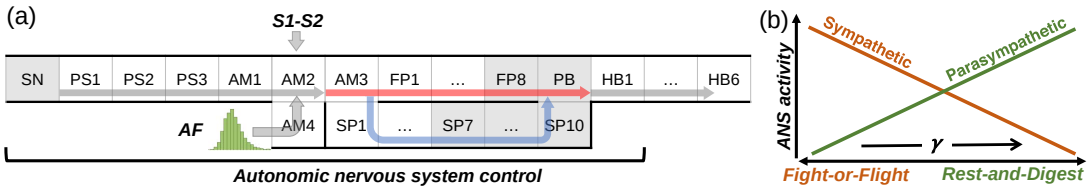

Figure 1. (a) Scheme of the rabbit AV node model. SN - sinus node, PS - peripheral sinus node, AM - atrial muscle, FP - fast pathway, SP - slow pathway, PB - penetrating bundle, and HB - His bundle cells. (b) Dynamic balance between the branches of autonomic nervous system.

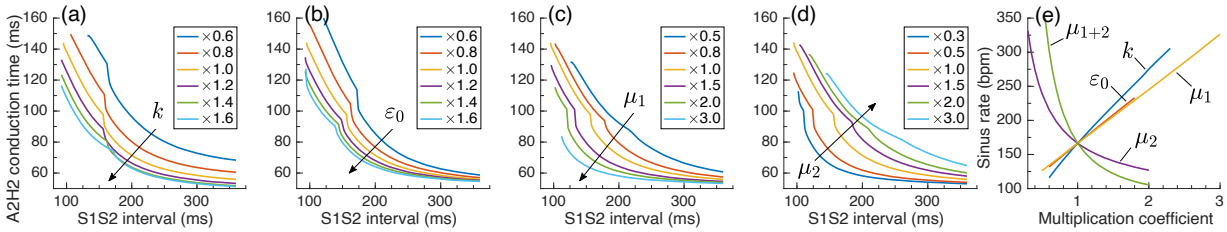

Figure 2. Influence of variation of the A-P model parameters (k, ε_0, μ_1, and μ_2) on the shape and position of conduction curve A2H2 (panels a-d) and sinus rate (e). Arrows indicate the increase of the multiplication coefficient.

demonstrated in Fig. 2. In the case of k, the reentrant activity existed with slower (higher) conduction curves in the range of dominating parasympathetic tone ($\gamma = 0.6-1.2$). It disappeared only at $\gamma > 1.2$ with faster conduction curves, i. e., at enhanced sympathetic tone [Fig. 2(a)]. For the variation of ε_0, the reentrant waves remain in the whole range of γ [Fig. 2(b)]. Hence, we concluded that the parameters k and ε_0 are unsuitable for mimicking ANS activity. On the other hand, with the variation of the parameters μ_1 and μ_2 responsible for cell refractoriness [7], the upper shift of the conduction curve [Figs. 2(c) and 2(d)] led to termination of any reentrant activity. We concluded that the combination of μ_1 and μ_2 best corresponds to the ANS tone effect on AV node reported in the literature [6, 9, 10]. Figure Fig. 2(e) shows the change of SN rate with varying multiplication coefficient for the A-P model parameters.

Thus, we implemented the effect of the ANS [Fig. 1(b)] in our model, applying the multiplication (ANS) coefficient γ simultaneously to the parameters μ_1 and μ_2: $\mu_1^* = \mu_1/\gamma$, $\mu_2^* = \mu_2\gamma$ [13]. For the sake of simplicity, the same coefficient γ was used in the model cells from SN to HB1, including AV junctional pacemaker cells [Fig. 1(a)].

3. Results and discussion

Simulated recovery (A2H2 conduction time vs S1S2 interval) and refractory (H1H2 conduction time vs S1S2 interval) curves for rabbit AV node with ANS control under premature atrial pacing are shown in Figs. 3 and 4. The anterograde conduction curves have an exponential-like shape with pronounced bending when conduction changes from FP to SP with a reduced S2 pacing interval [Fig. 3(a)]. This is essential for normal AV node operation under anterograde conduction, allowing effective conduction slowing and fast rhythm filtering, confirmed by experimental and simulation studies [1, 2, 5]. With increasing parasympathetic tone, the conduction curve bending becomes smoother and virtually disappears [Fig. 3(a)]; the ERP of SP [Figs. 3(b)] rises slower than ERP of FP [Fig. 3(c)], leading to an increase in the difference of their ERPs [Fig. 3(d)]. With increasing γ, the refractory curves shift up and right in control and ablation cases [Figs. 4(a)-4(c)], resulting in an increase of the difference in functional refractory periods (FRP) [Fig. 4(d)].

At atrial pacing, due to the significant difference between ERPs of SP and FP present in an intact AV node, only the typical slow-fast type AVNRT can be observed. The simulated ladder diagrams in Fig. 5(a) show that only a few echo beats appeared at $\gamma = 1.2$. Typical AVNRT was initiated with the premature atrial impulse at dominant sympathetic tone ($\gamma = 0.8$) and spontaneously terminated with the rise of parasympathetic tone at $\gamma > 1.1$. The strong short burst of sympathetic tone may also cause the onset of the same type of AVNRT [Fig. 5(b)].

We also considered the effect of ANS on the AV node filtering function during AF. For this purpose, we applied an atrial impulse series of $N_{\mathrm{A}} = 2000$ intervals using correlated Pearson IV type distribution with mean $M_{\mathrm{AA}} = 70$ ms, standard deviation $S_{\mathrm{AA}} = 12$ ms and obtained standard His-His (HH) histograms and bidimensional Poincaré plots in the wide range of ANS tones $\gamma = 0.8-2.0$. Figure 6 demonstrates simulation results of

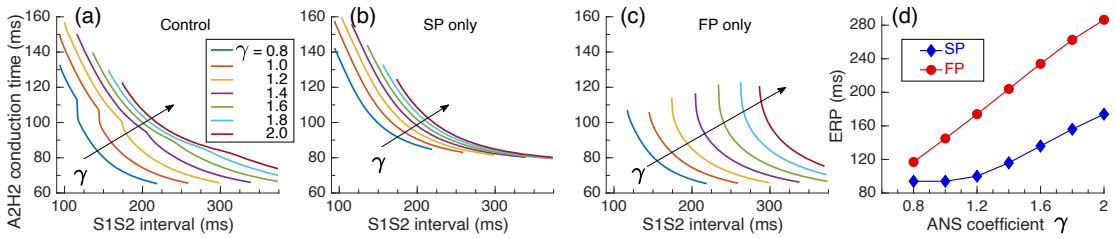

Figure 3. Anterograde recovery curves (A2H2): (a) Control, (b) FP ablation, (c) SP ablation. (d) SP (=Control) and FP effective refractory periods vs ANS coefficient γ.

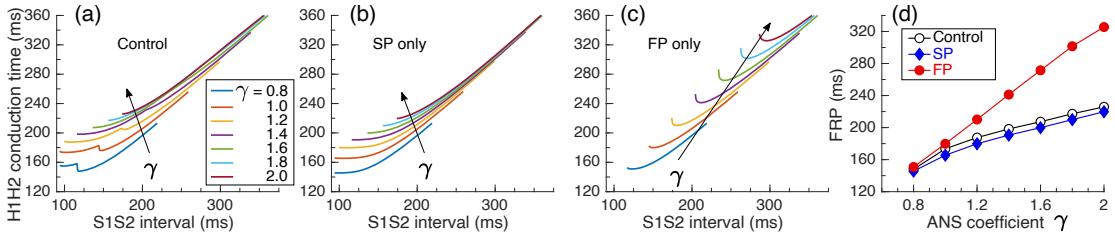

Figure 4. Anterograde refractory curves (H1H2): (a) Control, (b) FP ablation, (c) SP ablation. (d) Control, SP and FP functional refractory periods (FRP) vs ANS coefficient γ.

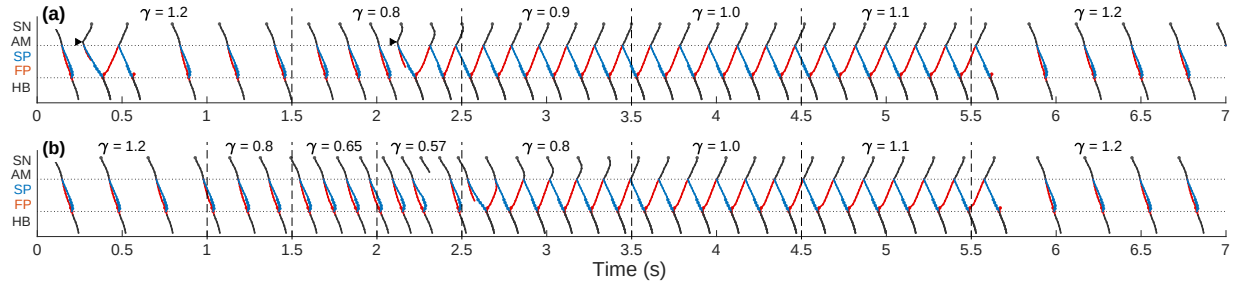

Figure 5. Calculated Lewis ladder diagrams of the excitation propagation in the AV nodal dual pathway structure from SN to HB through FP (red traces) and SP (blue traces). Black arrowheads denote places and moments of premature stimulation. (a) Onset of typical slow-fast AVNRT with atrial premature stimulation at enhanced sympathetic tone ($\gamma = 0.8$). (b) A short burst of high sympathetic tone with high sinus rhythm also caused typical AVNRT. With the rising vagal tone ($\gamma \geq 1.2$) the oscillations terminated spontaneously in both cases.

AV node filtering function during AF with changing ANS tone from strong sympathetic to strong parasympathetic ($\gamma = 0.8 - 2.0$). Unimodal and bimodal standard HH histograms were obtained both in control cases and in cases of SP ablation, which may indicate that the histogram shapes depend not on the number of active AV node pathways but mostly on the dominant tone of the ANS. After SP ablation, the mean HH intervals M_{HH} increased significantly [Fig. 6(b)], which is consistent with clinical observations.

4. Conclusion

We developed a model of the rabbit AV node incorporating control of the autonomic nervous system. The control is achieved by altering cell refractoriness using a single coefficient, resulting in changes in nodal conduction delays and intrinsic rate of pacemaker cells. The inclusion of sympathetic and parasympathetic tones in our model is qualitatively based on experimental data and clinical observations and manifests in the corresponding shifts of conduction curve. The ability of the modified model to reproduce the effect of the ANS on AV node function was illustrated by examples of the onset and spontaneous termination of AVNRT and changes in nodal filtering function during AF. The modified model represents a valuable tool for studying the AV node and opens new possibilities for understanding cardiac electrophysiology.

Acknowledgments

The work was supported by JSPS KAKENHI Grant No. 20K12046.

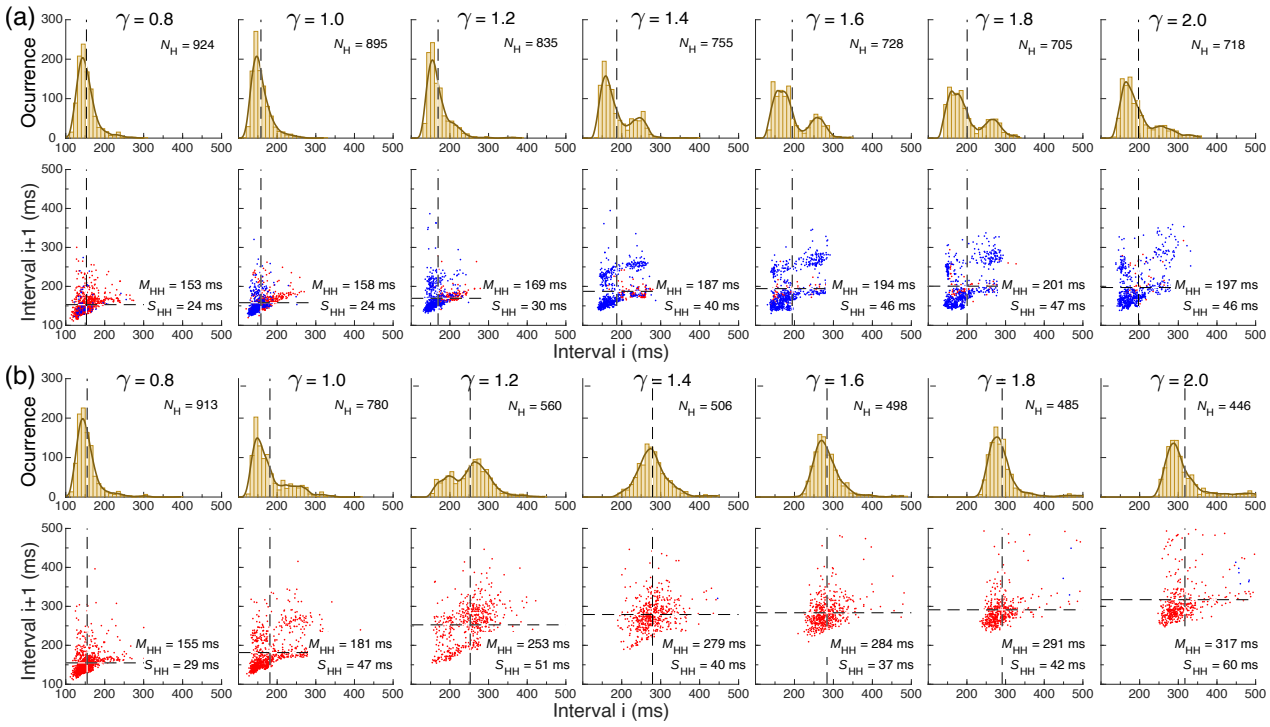

Figure 6. Standard HH histograms (top panels) and bidimensional Poincaré plots (bottom panels) calculated at different values of ANS coefficient γ. (a) Intact AV node, (b) SP ablation case. N_{H} is the number of beats passing His bundle, M_{HH} is the mean HH interval (marked also by the dashed lines), and S_{HH} is the standard deviation of HH intervals. Red dots correspond to the impulses entered His bundle through FP, blue - through SP.

References

[1] Inada S, Hancox JC, Zhang H, Boyett MR. One-dimensional mathematical model of the atrioventricular node including atrio-nodal, nodal, and nodal-His cells. Biophys J 2009;97:2117–2127.

[2] Climent AM, Guillem MS, Zhang Y, Millet J, Mazgalev TN. Functional mathematical model of dual pathway AV nodal conduction. Am J Physiol Heart Circ Physiol 2011;300:H1393–H1401.

[3] Plappert F, et al. An atrioventricular node model incorporating autonomic tone. Front Physiol 2022;13:Art. no. 976468.

[4] Ryzhii M, Ryzhii E. A compact multi-functional model of the rabbit atrioventricular node with dual pathways. Front Physiol 2023;14:Art. no. 1126648.

[5] Billette J, Tadros R. An integrated overview of AV node physiology. Pacing Clin Electrophysiol 2019;42(7):805–820.

[6] Manolis AA, et al. The role of the autonomic nervous system in cardiac arrhythmias: The neuro-cardiac axis, more foe than friend? Trends Cardiovasc Med 2021:31(5):290–302.

[7] Aliev RR, Panfilov AV. A simple two-variable model of cardiac excitation. Chaos Solitons Fractals 1996;7(3):293–301.

[8] Ryzhii M, Ryzhii E. Pacemaking function of two simplified cell models. PLoS ONE 2022;17(4):Art. no. e0257935.

[9] Nigro G, et al. Autonomic nervous system modulation before the onset of sustained atrioventricular nodal reentry tachycardia. Ann Noninvasive Electrocardiol 2010;15(1):49–55.

[10] Xiao L, et al. Combined modified Valsalva maneuver with adenosine supraventricular tachycardia: A comparative study. Am J Emerg Med 2024;78:157–162.

[11] Lin LJ, et al. Properties and substrate of slow pathway exposed with a compact node targeted fast pathway ablation in rabbit atrioventricular node. J Cardiovasc Electrophysiol 2001;12(4):479–86.

[12] Ryzhii M, Ryzhii E. Revealing the origin of typical and atypical forms of atrioventricular nodal reentrant tachycardia with a compact computer model of rabbit AV node. Computing in Cardiology (CinC) 2023;1–4.

[13] Ryzhii M, Ryzhii E. Atrioventricular nodal reentrant tachycardia onset, sustainability, and spontaneous termination in rabbit atrioventricular node model with autonomic nervous system control. bioRxiv 2024.06.10.598392.

Address for correspondence:

Maxim Ryzhii
University of Aizu
Aizu-Wakamatsu 965-8580, Japan
m-ryzhii @ u-aizu.ac.jp